THE ASTROPHYSICAL JOURNAL, 575:L25–L28, 2002 August 10

ELECTROSTATIC TURBULENCE AND DEBYE-SCALE STRUCTURES ASSOCIATED WITH ELECTRON THERMALIZATION AT COLLISIONLESS SHOCKS

S. D. BALE, A. HULL, D. E. LARSON, R. P. LIN,[1] AND L. MUSCHIETTI
Space Sciences Laboratory, University of California at Berkeley, MC 7450, Berkeley, CA 94720
AND
P. J. KELLOGG, K. GOETZ, AND S. J. MONSON
School of Physics and Astronomy, University of Minnesota, 116 Church Street, SE, Minneapolis, MN 55455
Received 2002 May 4; accepted 2002 July 1; published 2002 July 11

ABSTRACT

We analyze measurements of bipolar, Debye-scale electrostatic structures and turbulence measured in the transition region of the Earth's collisionless bow shock. In this region, the solar wind electron population is slowed and heated, and we show that this turbulence correlates well in amplitude with the measured electron temperature change. The observed bipolar structures are highly oblate and longitudinally polarized and may instantaneously carry up to 10% of the plasma energy $\psi \equiv e\phi/k_b T_e \approx 0.1$ before dissipating. The relationship between ψ and the field-aligned scale size $\Delta_\parallel$ of the Gaussian potential suggests that the bipolar structures are BGK trapped particle equilibria or electron hole modes. We suggest a generation scenario and a potential role in dissipation.

Subject headings: instabilities — shock waves — turbulence

1. INTRODUCTION

Collisionless shocks decelerate and thermalize a super-Alfvénic plasma flow in the absence of binary particle collisions. In the upstream (unshocked) to downstream (shocked) transition region, intense, broadband, electrostatic turbulence is observed (Rodriguez & Gurnett 1975; Onsager et al. 1989; Scudder et al. 1986) below the electron plasma frequency ω_{pe}. Spectral density measurements found a broad spectrum whose peak translated as $f_{\rm peak} \propto v_{\rm sw}/\lambda_{\rm D}$, where $v_{\rm sw}$ is the observed solar wind speed (Rodriguez & Gurnett 1975). Early theories of electron and ion heating at shocks invoked random-phase wave-particle scattering in this (presumed linear) wave field as a thermalization agent (Papadopoulos 1985), and hence the source of entropy, while more recent models of particle heating at shocks emphasize the effect of the macroscopic electric and magnetic fields.

In particular, at low Mach number shocks ($M \leq 10$) the electrons are thought to behave adiabatically in the shock transition layer, broadening in phase space as they move into the magnetic mirror and electric potential of the shock (Scudder 1995; Feldman et al. 1983; Hull et al. 1998). This reversible motion introduces regions of phase space that are inaccessible, which may provide free energy for a two-stream (electron-electron) instability (Gedalin 1999). At low Mach number shocks, the electrons are observed to receive approximately 25% of the available thermal energy [$\Delta T_e/(\Delta T_e + \Delta T_i) \approx 0.25$] (Thomsen et al. 1987). However, soft X-ray observations of thermal bremsstrahlung from young supernova remnant shocks, where Mach numbers are much higher ($M \approx 100$–1000), suggest the equipartition of thermal energy ($T_e \approx T_i$; McKee & Hollenbach 1980). Simulations of high Mach number shocks (Cargill & Papadopoulos 1988; Shimada & Hoshino 2000) indicate a two-step electron heating process: a Buneman instability operating between incoming electrons and the reflected ion population preheats the electrons until $T_e > T_i$, whereafter an ion acoustic instability draws energy from the streaming electrons and incoming ions to continue the heating. Such a process may continue heating to equipartition in high Mach number shocks; hence, an understanding of the nature of this instability is of interest.

In this Letter, we show that the electrostatic turbulence observed in the shock transition region is coherent and often composed of small-scale bipolar structures. We use the term "turbulence" to apply to the broadband spectrum of fluctuations, without otherwise specifying the form of the spectrum (e.g., power law). The wave amplitude is well correlated with the observed electron temperature change $\Delta T_e/T_e$ across the shock. Furthermore, we show that the observed bipolar structures are longitudinally polarized, highly oblate features with a scaling of electric potential with characteristic scale size $\psi = e\phi_0/k_b T_e \propto \Delta_\parallel$, where $\phi(x) = \phi_0 e^{-x^2/2\Delta_\parallel^2}$. These properties suggest that the observed structures may be one-dimensional BGK electron phase-space holes, as opposed to Korteweg–de Vries (KdV) solitons.

2. DATA

Measurements are made by the WAVES (Bougeret et al. 1995) and Three-Dimensional Plasma (3DP; Lin et al. 1995) experiments on the *Wind* spacecraft at 33 separate, predominantly quasi-perpendicular bow shock crossings. A waveform capture instrument (WAVES time domain sampler [TDS]) samples two orthogonal wire antennas of tip-to-tip lengths 100 and 15 m (X and Y, respectively) at 120,000 samples per second and buffers 17 ms "events." The buffered events are sorted by amplitude for delivery to the telemetry system; this introduces a selection effect whereby smaller amplitude events are displaced on the finite-length buffer; hence, data event occurrence is a proxy for voltage amplitude. This algorithm produced 108 waveform events at the 33 observed shocks. Electrostatic analyzer instruments (3DP/EESA-L and 3DP/PESA-L) measure three-dimensional electron and proton distributions over the 3 s spin period of the spacecraft. Particle density is calculated as an integral over the distribution, and particle thermal temperature is estimated from the second moment of the distribution. Electron distribution measurements have been corrected for spacecraft potential effects. Emitted pho-

[1] Also at Department of Physics, University of California at Berkeley, 366 LeConte Hall, Berkeley, CA 94720.

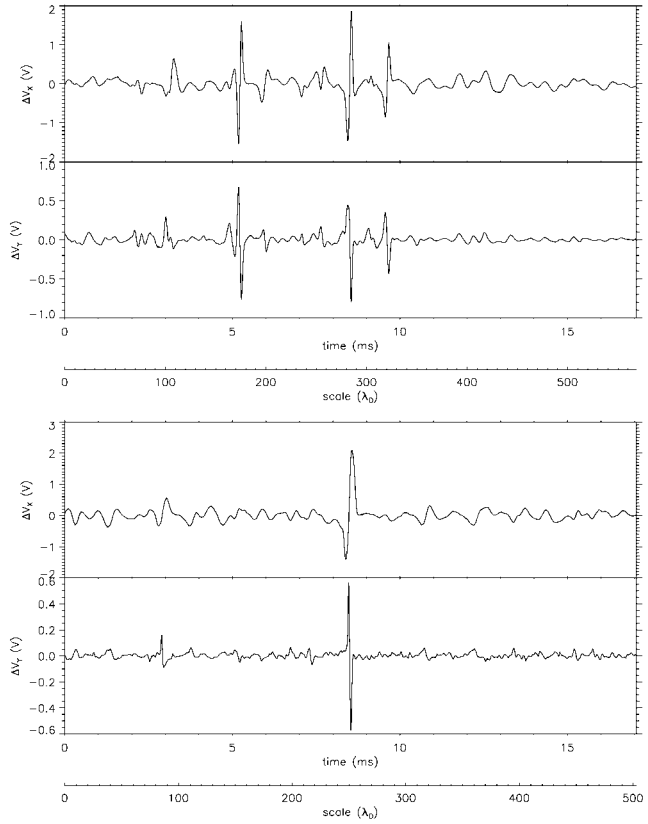

FIG. 1.—Antenna voltage measurements of electrostatic turbulence and structures on the bow shock ramp. Orthogonal *X*-*Y* measurements are shown for two events, as a function of time and convected solar wind distance ($\Delta x = v_{sw}\Delta t/\lambda_e$). Low-level turbulence and Debye-scale bipolar structures coexist in this region.

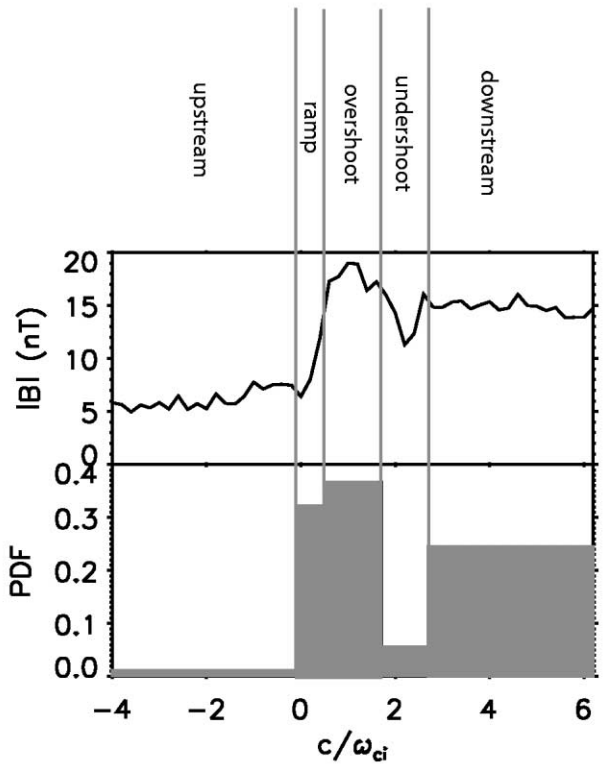

FIG. 2.—Probability distribution of waveform events, peaking in the shock ramp and overshoot. Observed shocks are indexed by upstream, ramp, overshoot, undershoot, and downstream regions and the occurrence of data events accumulated in these bins. The upper data panel shows the magnetic profile of a typical supercritical shock at 3 s time resolution, and the lower panel is the probability of occurrence of 108 events. The ordinate is given in ion inertial lengths assuming a ramp scale equal to $1c/\omega_{pi}$.

toelectrons cause the sunlit spacecraft to float positive relative to the plasma, which attracts a measured electron return current. Proton density measurements are used to estimate the spacecraft potential, and the measured electron distribution is corrected using Liouville's theorem. The data in Figure 1 are waveforms sampled on the magnetic ramp of the bow shock by the TDS instrument; *X* and *Y* antenna voltage measurements are shown in pairs. The upper pair shows individual bipolar spikes separated by several milliseconds, while the lower pair shows low-level turbulence with embedded bipolar spikes. The low-level (≈0.1 V), less localized turbulence also contributes to the observed power (Onsager et al. 1989) in the shock. An axis below each waveform pair is a convected scale length given by $\Delta x = (v_{sw}\Delta t)/\lambda_D$, where the solar wind speed v_{sw} and Debye length $\lambda_D = (k_b T_e/4\pi ne^2)^{1/2}$ are measured locally. In Figure 2, we accumulate the occurrence of waveform events as a function of position in the shock structure. The upper data panel shows the magnetic profile of a typical supercritical shock, exhibiting overshoot and undershoot features. The lower panel shows the region of occurrence of 108 waveform events at 33 separate shocks. The ordinate of this plot is distance in ion inertial lengths, calibrated to force the spatial scale of the ramp to $1c/\omega_{pi}$. The distribution is peaked in the shock ramp and overshoot, where the primary modification to the electron distribution also occurs. Since event occurrence indicates amplitude, this is the region of most intense turbulence. Note that the ramp is spatially much thinner than the overshoot; hence, the occurrence probability per unit length is higher there.

The bipolar structures can be seen to have a characteristic scale of several λ_D, as will be shown below. The bipolar voltage spikes are well modeled by the derivative of a Gaussian potential $\phi(x) = \phi_0 e^{-x^2/2\Delta_\parallel^2}$, and the voltage response of the antenna system has been shown to indicate a scale size consistent with that given by convection (Bale et al. 1998). In Figure 3, we show the relationship between the dimensionless potential $\psi = e\phi_0/k_b T_e$ and the Gaussian scale size $\Delta_\parallel$ in units of Debye length, where the potential amplitude ϕ_0 and scale size $\Delta_\parallel$ are determined by fitting the observations to the derivative of the potential. Open circles are the observed potentials. Filled circles are averages of potential and scale size within $1\lambda_D$ bins, with 1 σ error bars. Larger scales are seen to correspond to larger values of potential amplitude, the relationship is roughly linear, and a line $\psi = \beta\Delta_\parallel$ fitted through zero and to the averages gives $\beta \approx 0.016\lambda_D^{-1}$. Since the peak electric field occurs at the inflection points of the potential, $E_p = \exp^{-1/2}\phi_0/\Delta_\parallel$, which can be rewritten as $eE_p\lambda_D = 0.009k_b T_e$. Stabilization of a beam-driven instability occurs on the order of $\gamma\tau \approx 1$, where γ is the growth rate and τ is the trapping time $(m_e/eEk)^{1/2}$ (Papadopoulos et al. 1971). Furthermore, the electrons are thermalized after a few maximum growth periods $1/\gamma_{max} = (2/\sqrt{3})(4m_i/m_e)^{1/3}\omega_{pe}^{-1}$ (Davidson et al. 1970). Setting $\gamma_{max}\tau \approx 1$ gives, after some algebra, $eE\lambda_D = \frac{3}{4}(m_e/4m_i)^{1/3}k_b T_e \approx 0.002k_b T_e$. This excellent agreement with data implies that the linear relationship $eE_p\lambda_d \propto k_b T_e$ may simply indicate the saturation level of an instability.

Furthermore, the relationship $\partial\psi(\Delta)/\partial\Delta > 0$ is unlike that of KdV solitons, which arise from a competition between steepening and dispersion and have larger amplitude at smaller scales.

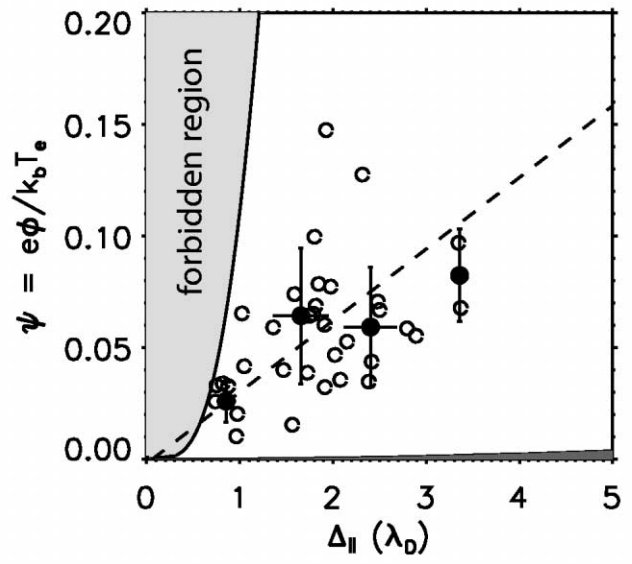

FIG. 3.—Peak dimensionless potential ψ vs. Gaussian scale size $\Delta_\parallel$ showing a linear trend of positive slope. This is consistent with BGK electron hole expectations and different from the focusing behavior of a KdV soliton. The gray shaded region at the left is the regime within which the distribution of trapped electrons becomes negative and no BGK solution is possible. The dark shaded region at very low ψ is the region of theoretical stability $\omega_b/\Omega_{ce} > 1$ developed for BGK modes in a plasma with small perpendicular temperature.

However, a similar relationship between potential and scale size has been observed in BGK electron phase space holes in auroral plasma (Ergun et al. 1998), although in that case the potential ψ is larger and appears to be limited by a stability criterion (Muschietti et al. 1999). Perturbations to the electron distribution consistent with the electron hole interpretation were observed in the auroral plasma (Ergun et al. 1998), where distribution function measurements are made on short timescales. However, our electron data are collected over one spin of the spacecraft (3 s), and perturbations on the millisecond timescale are impossible to recover. Our identification of the bipolar spikes as BGK electron holes rests on the scaling relationship of ψ increasing with $\Delta_\parallel$, the similarity to the auroral data, and the robust growth of electron holes in the late phase of simulations of two-stream and Buneman instabilities (Goldman, Oppenheim, & Newman 1999; Shimada & Hoshino 2000). Recent work (Muschietti et al. 2000) has shown that electron holes may be unstable to transverse fluctuations when the electron bounce frequency exceeds the cyclotron frequency $\omega_b > \omega_{ce}$, where $\omega_b/\omega_{pe} = (\psi/\Delta_\parallel^2)^{1/2}$. The dark shaded region at the bottom of Figure 3 shows that condition for our data and implies that our events exist in the domain of instability. However, this condition may not apply in the more isotropic electron environment of a shock. Indeed, it was suggested Muschietti et al. (2000) that the transverse instability requires a narrow perpendicular thermal velocity spread $v_{\perp e} \ll \omega_b/k$ so that trapped electrons do not disperse during one traversal of the potential. This condition can be written $v_{\perp e}/v_e \ll \psi/8\pi^2$ and is not met in our data, where $v_{\perp e}/v_e$ is of order 1. The gray shaded region on the left of Figure 3 shows the parameter space within which the electron holes cannot exist; in this regime, the distribution of trapped electrons becomes negative. Again, our data exist in a domain of stability.

The antenna response to the potential structure is a function of the Gaussian scale size Δ relative to the antenna. Structures of a few Debye lengths are typically 10–100 m, while the two wire antennas are 15 and 100 m tip to tip. This intermediate

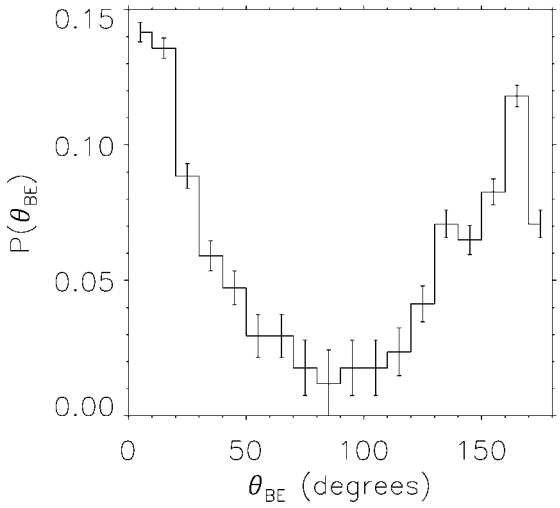

FIG. 4.—Histogram of antenna-magnetic field angle. Event occurrence is a proxy for voltage amplitude, and peak occurrence is when the wire antennas are roughly aligned with the local magnetic field direction. Hence, the wave electric field vector is roughly parallel to the magnetic field, indicating a structure with a large perpendicular wavelength.

scale gives a different response on each wire (Bale et al. 1998). Simply, potential structures larger than the long antenna (100 m) will give antenna responses in the ratio of antenna physical lengths (100 m/15 m $\approx$ 6.67), while it can be seen in Figure 1 that the ratio of response for these data is smaller. Since event occurrence indicates amplitude, and only the long wire (100 m) is used to trigger the TDS instrument, we can accumulate statistics to give polarization information. When the voltage signal on the two antennas is in phase, we assign the wave electric field vector to lie in a particular quadrant (with 180° ambiguity); if the signals are out of phase, we assign the vector to an adjacent quadrant (again $\pm 180°$ ambiguous). Figure 4 is a histogram of occurrence of the angle between the center of the appropriate quadrant and the projection of the local magnetic field direction into the plane of the antennas. The histogram is strongly peaked

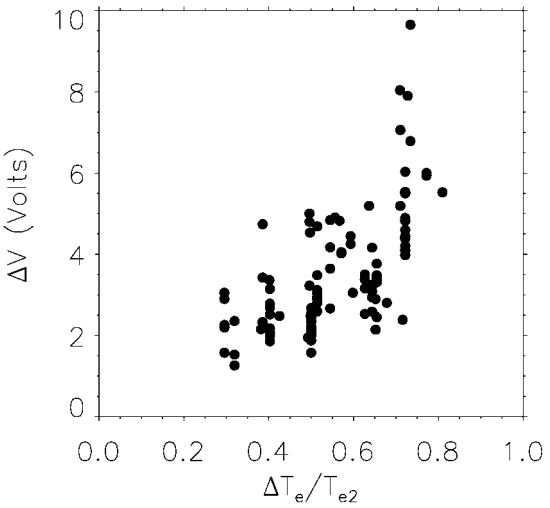

FIG. 5.—Turbulent voltage amplitude as a function of observed electron temperature change $\Delta T_e/T_{e2} = (T_{e2} - T_{e1})/T_{e2}$. Largest observed wave fields occur for a large electron temperature jump. Since $\Delta T_e/T_{e2}$ may be a proxy for the shock dHT potential $\Delta\Phi_{HT}$, this indicates a large modification to the electron distribution function by shock DC fields, which may then be unstable.

at 0° and 180°, indicating that the wave electric field vector is directed primarily along the local magnetic field. For the bipolar structures, this implies an oblate, pancake-shaped object with a Debye-scale Gaussian potential along $\boldsymbol{B}$ and larger perpendicular dimension. This is consistent with magnetospheric observations of BGK modes (Franz et al. 2000), which extrapolate to large oblateness at our average frequency ratio $\Omega_{ce}/\omega_{pe} \approx 1/80$. Figure 5 shows the measured peak voltage amplitude in each waveform event as a function of the measured electron temperature change across the shock $\Delta T/T_{e2} = (T_{e2} - T_{e1})/T_{e2}$, where T_{e2} and T_{e1} are the downstream (shocked) and upstream (unshocked) temperatures, respectively. In the case that fluid closure is achieved with an electron polytrope law $p_e \propto n_e^{\gamma_e}$, the shock de Hoffman–Teller (dHT) potential $\Delta\Phi_{\rm HT}$ is found to be proportional to the electron temperature change (for $\gamma_e \neq 1$), and hence ΔT is a proxy for $\Delta\Phi_{\rm HT}$. It is the dHT potential that excludes low-energy ($E_\parallel \leq \Delta\Phi_{\rm HT}$) electrons from the transition region.

3. DISCUSSION

The correlation of temperature change with voltage amplitude of the electrostatic turbulence might be taken as an indication of electron heating by the turbulence. However, given the probable effects of the macroscopic fields, it is likely that the correlation is one with the cross-shock dHT potential. Large dHT potentials indicate large modifications to the electron distribution function, which may then be unstable to the growth of a beam mode in the shock ramp. This beam mode then grows to a nonlinear state, including the formation of the electron hole structures and eventual thermalization, or velocity-space mixing, of the electrons. Particle simulations (Shimada & Hoshino 2000) show electron and ion heating associated with electron hole formation in the upper range of our Mach number regime ($M_{\rm A} \approx 10$), which may point to enhanced heating at very high Mach numbers.

Work on the *Wind* spacecraft is supported at University of California at Berkeley by NASA grants NAG5-2815 and NAG5-7691 to the University of California.

REFERENCES

Bale, S. D., Kellogg, P. J., Larson, D. E., Lin, R. P., Goetz, K., & Lepping, R. P. 1998, Geophys. Res. Lett., 25, 2929
Bougeret, J.-L., et al. 1995, Space Sci. Rev., 71, 231
Cargill, P. J., & Papadopoulos, K. 1988, ApJ, 329, L29
Davidson, R. C., Krall, N. A., Papadopoulos, K., & Shanny, R. 1970, Phys. Rev. Lett., 24, 579
Ergun, R. E., Carlson, C. W., McFadden, J. P., Mozer, F. S., Muschietti, L., Roth, I., & Strangeway, R. J. 1998, Phys. Rev. Lett., 81, 826
Feldman, W. C., et al. 1983, J. Geophys. Res., 88, 96
Franz, J. R., Kintner, P. M., Seyler, C. E., Pickett, J. S., & Scudder, J. D. 2000, Geophys. Res. Lett., 27, 169
Gedalin, M. 1999, Geophys. Res. Lett., 26, 1239
Goldman, M. V., Oppenheim, M. M., & Newman, D. L. 1999, Geophys. Res. Lett., 26, 1821
Hull, A. J., Scudder, J. D., Frank, L. A., Paterson, W. R., & Kivelson, M. G. 1998, J. Geophys. Res., 103, 2041
Lin, R. P., et al. 1995, Space Sci. Rev., 71, 125
McKee, C. F., & Hollenbach, D. J. 1980, ARA&A, 18, 219
Muschietti, L., Ergun, R. E., Roth, I., & Carlson, C. W. 1999, Geophys. Res. Lett., 26, 1093
Muschietti, L., Roth, I., Carlson, C. W., & Ergun, R. E. 2000, Phys. Rev. Lett., 85, 94
Onsager, T. G., Holzworth, R. H., Koons, H. C., Bauer, O. H., Gurnett, D. A., Anderson, R. R., Luhr, H., & Carlson, C. W. 1989, J. Geophys. Res., 94, 13,397
Papadopoulos, K. 1985, in Collisionless Shocks in the Heliosphere, ed. B. T. Tsurutani & R. G. Stone (Geophys. Monogr. 35; Washington, DC; AGU), 59
Papadopoulos, K., Davidson, R. C., Dawson, J. M., Haber, I., Hammer, D. A., Krall, N. A., & Shanny, R. 1971, Phys. Fluids, 14, 849
Rodriguez, P., & Gurnett, D. A. 1975, J. Geophys. Res., 80, 19
Scudder, J. D. 1995, Adv. Space Res., 15, 181
Scudder, J. D., Mangeney, A., Lacombe, C., Harvey, C. C., Wu, C. S., & Anderson, R. R. 1986, J. Geophys. Res., 91, 11,075
Shimada, N., & Hoshino, M. 2000, ApJ, 543, L67
Thomsen, M. F., Mellott, M. M., Stansberry, J. A., Bame, S. J., Gosling, J. T., & Russell, C. T. 1987, J. Geophys. Res., 92, 10,119